Electrophysiological–Metabolic Modeling of Microbes: Applications in Fuel Cells and Environment Analysis

Max Fontus and Peter Ortoleva

Abstract

A formalism for simulating coupled metabolic and electrophysiological processes is presented. The resulting chemical kinetic and electrophysiological equations are solved numerically to create a cell simulator. Metabolic features of this simulator were adapted from *Karyote*, a multi-compartment biochemical cell modeling simulator. We present the mathematical formalism and its computational implementation as an integrated electrophysiological-metabolic model. Applications to *Geobacter sulfurreducens* in the environment and in a fuel cell are discussed.

Key words: Cell modeling, E-Ms, Microbial fuel cell, Microbe–mineral interaction

1. Introduction

The coupling of electrophysiological and metabolic processes underlies many cellular phenomena. While there are many cell models that account for biochemistry, membrane potential, transport, and other processes, there is a need for a simulator that accounts for all these processes and their coupling with general stoichiometry and transport rate laws. There is also a model needed that takes into consideration the hierarchical structure of Eukaryotic cells, i.e., compartments within compartments. A brief review of cellular metabolomics and electrophysiological modeling is provided before presenting the integrated electrophysiological-metabolic (E-M) approach.

The metabolic network is a collection of biochemical reactions where outputs from one reaction are inputs to others; this network underlies the response of the metabolome. Metabolic modeling started with studies on glycolysis (1–4). Rate constants for such chemical kinetic models were calibrated using experimentally measured metabolite concentration data. There are many chemical

kinetic models for simulating the dynamics of biochemical processes in cells (5–9). *Karyote* is a compartmented hierarchical simulator (10, 11) that forms the basis of the metabolic facet of the present E-M approach. However, *Karyote* does not account for electrophysiological processes. The transport of charged species affects and is affected by the membrane potential, underlying a key feedback in the network of cellular processes. Since there are many systems where membrane potentials have been measured, a next logical step in cell modeling is an integrated E-M approach, thereby accounting for the coupling of metabolomic phenomena with electrophysiological ones.

Membrane potentials are involved in a vast array of metabolic activities from nutrient transport to cell motility and cognitive processes. Electrical potentials are known to play a key role in early development at the single cell stage (12) and even during late development and adult behavior (13). Thus, for a broad spectrum of processes from development to metabolism, the electrical aspect of cellular behavior must be considered.

Membrane potentials were traditionally measured with electrodes, but NMR has also been used in an indirect approach that has the advantage of being applicable to small cells or intracellular compartments (14, 15). The distribution of radiolabeled ions is also used to estimate membrane potentials (16). These techniques provide a rich set of electrophysiological data for developing and calibrating E-M models.

Membrane potentials are observed in a wide range of cell types, some of which are as follows (a list that is meant to be suggestive rather than comprehensive):

- Atrial cells (17)
- Red blood cells (18)
- Glial cells (19)
- Neutrophils (20)
- Pulmonary arterial smooth muscle cells (21)
- Myelinated axons (22)
- Embryonic ventricular myocytes (23)
- Coronary arterial cells (24)
- Hair cells (25)
- Melanotrophs (26)
- Squid Schwann cells (27)
- Paramecia (28)
- *Trypanosoma brucei* (29)
- Yeast spheroplasts (28)
- Bacteria (28, 30)

Bernstein proposed the first quantitative formulation for the origin of membrane potentials in terms of the properties of electrolytic solutions (31, 32). The theory was advanced by Goldman (33) who solved the Nernst–Planck equation for a membrane by assuming a constant electrical field. According to this development, the transmembrane flux of an ion depends only on the permeability, the membrane potential, and the aqueous concentration of that ion on each side of the membrane. The flux of each ion was taken to be independent of that for others. From this, the Goldman–Hodgkin–Katz formula for the membrane potential was derived. It does not hold for membranes wherein ion pumps and other transmembrane processes are active.

The Hodgkin–Huxley model is a set of nonlinear differential equations that approximate the electrical characteristics of excitable cells such as neurons and cardiac myocytes (33). Most bioelectrochemical models are extensions of this model (34). More comprehensive modeling of E-M phenomena involves several challenges. Because local deviations from charge neutrality cause large electrical forces, only biochemical reactions which balance charge should be used. Many cofactors necessary for intracellular enzyme-catalyzed reactions and signaling processes are ions (e.g., Mg^{2+} and Ca^{2+}) and thus E-M processes can be strongly coupled. Transport of H^+ across membranes affects pH which mediates many biochemical reactions. The model presented here is built on a formalism for simulating the aforementioned E-M processes.

Strong Coulomb forces tend to impose charge neutrality in an electrolyte solution. Thus, charge neutrality is maintained in most regions of the cell interior. The question arises as to the distribution of molecules between regions close and far from external and internal membranes. Thus, the flux across a membrane bounding the cell exterior or an internal compartment is distributed between contributions to the near-membrane and interior regions. This implies that the flux splits into a charge-neutral contribution and one that accounts for exchange with the Debye layers adjacent to the membranes. We address this via a novel electrochemical reaction-transport formalism.

2. Materials

Algorithm and computational approach
The E-M cell simulator accounts for general reaction stoichiometry for both the bulk medium and transmembrane processes. The implementation is hierarchical, i.e., compartments within compartments are allowed, and all possible connectivities between compartments are accounted for. Simulation times depend on the number of species and subcellular compartments. A typical run time is one

CPU hour for a 30-biological hour simulation involving hundreds of species and half-dozen compartments.

The governing equations presented in Subheading 3 are solved numerically using methods presented earlier (35). To address the typically wide separation of timescales, the DVODE stiff solver is used (36–41). The E-M software is an extension of the *Karyote* model (sysbio.indiana.edu/sysbio/karyote). The input data for the biochemical facet of E-M modeling is the same as for *Karyote*. This includes geometric information specifying the volume of each compartment and the areas of membranes separating each of them from their neighbors. These surface areas are multiplied by flux rates computed dynamically to reflect the changing conditions on either side of a membrane. The compartment in which a given reaction operates must be specified. Transmembrane processes involve reactants on either side of a membrane so that the membrane and the compartment in which each participating molecular species resides must be specified. Active membrane transport involves molecular species on both sides of a membrane. Intramembrane reactions and species can be modeled by introducing an associated intramembrane compartment and "membranes" separating the intramembrane zone from its surrounding compartments. With all molecular species, one must provide a charge; all reactions must be charge balanced and thus not provided in schematic form.

The *Karyote* E-M software used is free open-source and can be obtained by contacting the corresponding author. The *Karyote* website allows online use of the original version of *Karyote* that does not account for the E-M model described here. An online E-M version will be provided in the near future.

3. Methods

3.1. Compartmentalized Reaction-Transport Model

The cell is divided into N_c compartments labeled $\alpha = 1, \ldots, N_c$. The molecular species are labeled $i = 1, \ldots, N$; $c_{i\alpha}$ and [species i]$_\alpha$ denote the concentration and activity of species i in compartment α, respectively. Concentrations and electrical potentials are taken to be spatially uniform within a given compartment (except for a thin boundary layer as discussed below). Conservation of mass implies

$$\Omega_\alpha \frac{\mathrm{d}c_{i\alpha}}{\mathrm{d}t} = \sum_{\alpha' \neq \alpha}^{N_c} A_{\alpha/\alpha'} \tilde{J}_{i\alpha/\alpha'} + \Omega_\alpha \sum_{k=1}^{N_r} v_{ik\alpha} W_{k\alpha}, \tag{1}$$

where

$\tilde{J}_{i\alpha/\alpha'}$ = charge-neutral flux of i from the interior of α' to that of α (see below for further discussion)

$A_{\alpha/\alpha'}$ = area of the membrane separating α from α'

Ω_α = volume of α

$W_{k\alpha}$ = rate of reaction k in α

$v_{ik\alpha}$ = stoichiometric coefficient of species i for reaction k in α

The rate $W_{k\alpha}$ is taken to be in the form

$$W_{k\alpha} = R_{k\alpha}[e^{\Upsilon_{k\alpha}/RT} - 1]. \tag{2}$$

The reverse rate $R_{k\alpha}$ is taken to be in mass action form while the affinity $\Upsilon_{k\alpha}$ is given by

$$\Upsilon_{k\alpha} = \sum_{i=1}^{N} v_{ik\alpha}\mu_{i\alpha} \tag{3}$$

for electrochemical potential $\mu_{i\alpha}$. The electrochemical potentials are written in the form

$$\mu_{i\alpha} = \mu_{i\alpha}^o + RT \ln a_{i\alpha} + z_i F V_\alpha, \tag{4}$$

where $\mu_{i\alpha}^o$ is the reference chemical potential of species i in α. The membrane flux $J_{i\alpha/\alpha'}$ is divided into passive and deviatoric contributions:

$$J_{i\alpha/\alpha'} = h_{i\alpha/\alpha'} E_{i\alpha/\alpha'} + J_{i\alpha/\alpha'}^{act} \tag{5}$$

for permeability $h_{i\alpha/\alpha'}$, and equilibrium factor $E_{i\alpha/\alpha'}$ that vanishes with $\mu_{i\alpha} - \mu_{i\alpha'}$; $E_{i\alpha/\alpha'}$ is given by

$$E_{i\alpha/\alpha'} = q_{i\alpha/\alpha'} \left(\frac{[\text{species } i]_\alpha - [\text{species } i]_{\alpha'} e^{q_{i\alpha/\alpha'} L_{\alpha/\alpha'}}}{1 - e^{q_{i\alpha/\alpha'} L_{\alpha/\alpha'}}} \right), \tag{6}$$

where

$$q_{i\alpha/\alpha'} = F z_i (V_\alpha - V_{\alpha'}) / L_{\alpha/\alpha'} RT, \tag{7}$$

F = Faraday's constant

z_i = Valence of i

V_α = Electrical potential in α

$L_{\alpha/\alpha'}$ = Thickness of the membrane separating α and α'

This passive flux law is obtained by solving the Nernst–Planck equation assuming the electrical field is constant within the membrane. The formula for $E_{i\alpha/\alpha'}$ reduces to that used earlier for uncharged molecular species (10). $J_{i\alpha/\alpha'}^{\text{act}}$ is the contribution to the flux arising from active processes.

3.2. Electrophysiological Model

Consider a physical picture wherein a compartment is divided into the interior domain and a thin charged layer along the surface of the surrounding membrane. Within a compartment interior, charge neutrality,

$$\sum_{i=1}^{N} z_i c_{i\alpha} = 0 \tag{8}$$

is maintained (as can be shown via an asymptotic analysis of the continuum coupled reaction-transport-Poisson equations (42)). When ions emerge from one side of a membrane, they have one of two destinations, i.e., the charged boundary layer or the charge-neutral compartment interior. Recall $J_{i\alpha/\alpha'}$ is the total transmembrane flux of species i from α' to α. In vector form $F\underline{z} \cdot \underline{\tilde{J}}\alpha/\alpha'$ is the electrical flux from α' to α. A modified flux $\tilde{J}_{i\alpha/\alpha'}$ is defined to be the flux of species i that is transferred from the interior of α' to that of α, and is designed to not transfer net charge as follows. With this, the charge-neutral flux is given by

$$\underline{\widetilde{J}}_{\alpha/\alpha'} = \underline{J}_{\alpha/\alpha'} - \underline{z}_{mob,\alpha/\alpha'} \frac{\underline{z}_{mob,\alpha/\alpha'} \bullet \underline{J}_{mob,\alpha/\alpha'}}{\underline{z}_{mob,\alpha/\alpha'} \bullet \underline{z}_{mob,\alpha/\alpha'}}. \tag{9}$$

Here $\underline{z}_{mob,\alpha/\alpha'}$ is the vector of valences of the species that can transfer between compartment α' and α. Note that $\underline{z}_{mob,\alpha/\alpha'}$ and $\underline{J}_{\alpha/\alpha'}$ are N-dimensional vectors, constructed such that the components for the species that cannot traverse the $\alpha\alpha'$ membrane are zero. It can be verified that $\underline{z} \cdot \underline{\tilde{J}}_{\alpha/\alpha'} = 0$ (i.e., the current due to the charge-neutral flux of the ionic species able to traverse the $\alpha\alpha'$ membrane is zero). Hence, $\underline{\tilde{J}}_{\alpha/\alpha'}$ is the flux to use in the reaction-transport Eq. (1); it accounts for the mass transfer between the interior zones beyond the charged boundary layers. This guarantees that if $\underline{z} \bullet \underline{c}_{\alpha} = 0$ initially in all compartments then it will remain so always.

Consider the charging of the boundary layers surrounding a membrane. From the above, $FA_{\alpha/\alpha'}\underline{z} \bullet \underline{J}_{\alpha/\alpha'}$ is the net electrical current into α from α'. If $\sigma_{\alpha/\alpha'}$ is the charge/area on the α side of the $\alpha\alpha'$ membrane, then $\sigma_{\alpha/\alpha'} = -\sigma_{\alpha'/\alpha}$; this follows because strong Coulomb forces ensure that the oppositely charged layers on either side of the $\alpha\alpha'$ membrane balance (otherwise the boundary charge would redistribute to ensure this balance). With this, conservation of charge implies

$$\sum_{\alpha' \neq \alpha} A_{\alpha/\alpha'}\underline{z} \bullet \underline{J}_{\alpha/\alpha'} = \sum_{\alpha' \neq \alpha} A_{\alpha/\alpha'} \frac{d\sigma_{\alpha/\alpha'}}{dt}. \tag{10}$$

Assuming that capacitance $C_{\alpha/\alpha'}$ relates the membrane potential $V(V_{\alpha/\alpha'} = V_\alpha - V_{\alpha'})$, one has

$$F\sum_{\alpha' \neq \alpha} A_{\alpha/\alpha'}\underline{z} \bullet \underline{J}_{\alpha/\alpha'} = \sum_{\alpha' \neq \alpha} A_{\alpha/\alpha'} C_{\alpha/\alpha'} \frac{dV_{\alpha/\alpha'}}{dt}. \tag{11}$$

This constitutes a set of coupled differential equations for the potentials V_α in each compartment. Thus, one arrives at a set of $N + 1$ equations for the $N + 1$ variables in each compartment interior.

The convention that the potential is zero in the medium in which the system is immersed completes the electrophysiological model.

It might be stated that charge-preserving exchanges of ions between the charge boundary layer and the compartments interior could take place. For example, Ca^{2+} could exchange with two Na^+ or an Mg^{2+}, a process which is not accounted for. However, the boundary layer is only the thickness of the Debye length (a few angstroms in most intracellular environments) and thereby its contribution to overall mass balance for a given compartment is not significant. However, the above partitioning of charge keeps track of the net charge in these layers and thus the membrane potential is properly computed.

3.3. Transmembrane Process Rates

Macromolecules embedded in membranes play a central role in the functioning of a cell. Some of these macromolecules mediate the pumping of ions across a membrane up a chemical potential gradient. They also introduce highly nonlinear passive transport laws that imply favored directions for selected molecules (i.e., import or export) for a given compartment where they participate in particular reactions. Another group of membrane-bound macromolecules mediate processes wherein reactants on one side of a membrane yield products on the other. An example of such a macromolecule is the enzyme glycerol-3-phosphate oxidase that is embedded in mitochondrial membrane. In summary, selective and nonlinear membrane processes play a central role in creating and maintaining the viability and spatial organization of a cell. It is now shown how these membrane reaction and transport processes are accounted for in the present compartmentalized cell model.

The pumping of ions and other active transport across a membrane illustrates how such processes are accounted for in our reaction formulation. Consider a process in a membrane separating compartments α and α' such that for each of the N species

$$\sum_{i=1}^{N} [\xi_{i\alpha/\alpha'}(\text{species } i \text{ in } \alpha) + \tilde{\xi}_{i\alpha/\alpha'}(\text{species } i \text{ in } \alpha')] = 0. \quad (12)$$

The stoichiometric coefficients $\xi_{i\alpha/\alpha'}$ and $\tilde{\xi}_{i\alpha/\alpha'}$ are defined as follows. If $\xi_{i\alpha/\alpha'} > 0$ then $\xi_{i\alpha/\alpha'}$ i-type molecules appear in compartment α; if $\xi_{i\alpha/\alpha'} < 0$ then $\xi_{i\alpha/\alpha'}$ i-type molecules are removed from compartment α as a result of this process. The $\tilde{\xi}_{i\alpha/\alpha'}$ terms are similar except for i-type molecules in compartment α'. As an example, consider a proton pump for a membrane separating a mitochondrion from the cytosol:

$$H^+(\text{cyto}) + ATP^{4-}(\text{cyto}) \rightarrow H^+(\text{mito}) + ADP^{3-}(\text{cyto}) + Pi^-(\text{cyto})$$

$$(13)$$
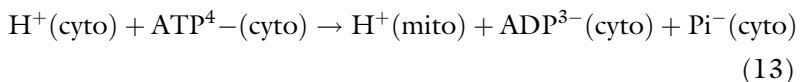
where P_i is inorganic phosphate. Thus, we have $\xi_{H^+cyto/mito} = -1, \tilde{\xi}_{H^+cyto/mito} = 1, \xi_{ATP^{4-}cyto/mito} = -1$, $\xi_{ADP^{3-}cyto/mito} = \xi_{P_icyto/mito} = 1$. With this, the flux $J_{cyto/mito}$ takes the form

$$J_{cyto/mito} = k[H^+]_{cyto}[ATP^{4-}]_{cyto} \tag{14}$$

for rate coefficient k. The process has been assumed to be irreversible and, for simplicity, $[\cdots]$ implies concentration here. More general process rate laws can also be used, e.g.,

$$J_{\alpha/\alpha'} = k \prod_{\xi_{j\alpha/\alpha'} < 0} [\text{species } j]_\alpha^{-\xi_{j\alpha/\alpha'}} \prod_{\xi_{j\alpha/\alpha'} < 0} [\text{species } j]_{\alpha'}^{-\tilde{\xi}_{j\alpha/\alpha'}}. \tag{15}$$

With this, the system evolves via

$$\Omega_\alpha \frac{dc_{i\alpha}}{dt} = A_{\alpha/\alpha'}(\xi_{i\alpha/\alpha'}\tilde{J}_{\alpha/\alpha'}) + \text{other terms}. \tag{16}$$

A common cellular feature is the Na^+/K^+-exchange pump. For example, consider the process

$$3Na^+(\alpha) + 2K^+(\alpha') + ATP^{4-}(\alpha)$$
$$\to 2K^+(\alpha) + 3Na^+(\alpha') + ADP^{3-}(\alpha) + Pi^-(\alpha) \tag{17}$$
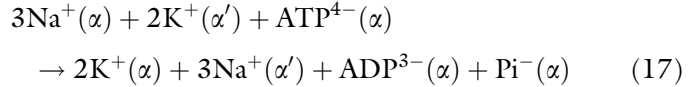
In this case, the flux law becomes

$$J_{\alpha/\alpha'} = k[Na^+]_\alpha^3[K^+]_{\alpha'}^2[ATP^{4-}]_\alpha. \tag{18}$$

The rate coefficients depend on the number of pump macromolecules per membrane area.

3.4. Geobacter in the Environment

Prokaryotic cells are used in this and the following section to demonstrate E-M modeling. Observed phenomena exhibited by such cells include the following:

- Membrane potentials
- Active and passive transmembrane fluxes
- Internal biochemical reactions
- Processes involving reactions and products on both sides of the membrane
- Precipitation of organic particles within the cell for internal substrate storage
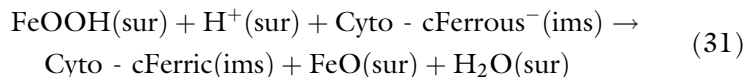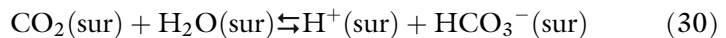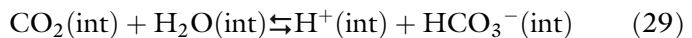- Transfer of electrons from the interior to reduce oxidized minerals in the surroundings
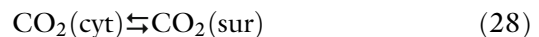
The objective of this section is to demonstrate that our E-M methodology integrates all such processes into a self-consistent model. We illustrate how the interaction of a bacterium with oxidized mineral grains in the surroundings and a source of reduced
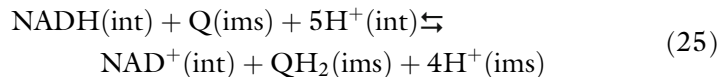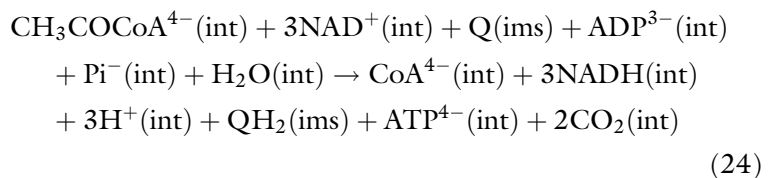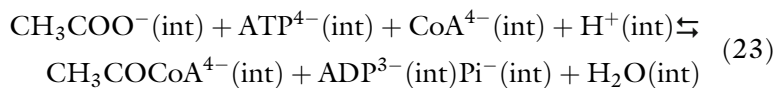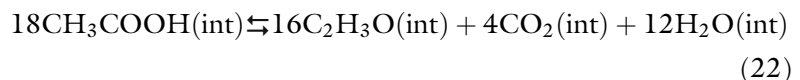
organic molecules can drive ATP production and energy storage processes fundamental to the functioning of these cells.

The system is divided into three compartments: surroundings (sur), interior zone (int), and the intramembrane space between the interior zone and the outer membrane of the microbe (ims).

The reactions and the compartments in which they are operating are as follows:

$$CH_3COOH(sur) \leftrightarrows CH_3COO^-(sur) + H^+(sur) \quad (19)$$

$$CH_3COOH(int) \leftrightarrows CH_3COO^-(int) + H^+(int) \quad (20)$$

$$CH_3COOH(sur) \leftrightarrows CH_3COOH(int) \quad (21)$$

$$18CH_3COOH(int) \leftrightarrows 16C_2H_3O(int) + 4CO_2(int) + 12H_2O(int) \quad (22)$$

$$CH_3COO^-(int) + ATP^{4-}(int) + CoA^{4-}(int) + H^+(int) \leftrightarrows$$
$$CH_3COCoA^{4-}(int) + ADP^{3-}(int)Pi^-(int) + H_2O(int) \quad (23)$$

$$CH_3COCoA^{4-}(int) + 3NAD^+(int) + Q(ims) + ADP^{3-}(int)$$
$$+ Pi^-(int) + H_2O(int) \rightarrow CoA^{4-}(int) + 3NADH(int)$$
$$+ 3H^+(int) + QH_2(ims) + ATP^{4-}(int) + 2CO_2(int) \quad (24)$$

$$NADH(int) + Q(ims) + 5H^+(int) \leftrightarrows$$
$$NAD^+(int) + QH_2(ims) + 4H^+(ims) \quad (25)$$

$$ATP^{4-}(int) + H^+(int) \rightarrow ADP^{3-}(int) + Pi^-(int) + 2H^+(ims) \quad (26)$$

$$QH_2(ims) + 2Cyto\text{-}cFerric(ims) + 2H^+(int) \rightarrow$$
$$Q(ims) + 2Cyto\text{-}cFerrous^-(ims) + 4H^+(ims) \quad (27)$$

$$CO_2(cyt) \leftrightarrows CO_2(sur) \quad (28)$$

$$CO_2(int) + H_2O(int) \leftrightarrows H^+(int) + HCO_3^-(int) \quad (29)$$

$$CO_2(sur) + H_2O(sur) \leftrightarrows H^+(sur) + HCO_3^-(sur) \quad (30)$$

$$FeOOH(sur) + H^+(sur) + Cyto\text{-}cFerrous^-(ims) \rightarrow$$
$$Cyto\text{-}cFerric(ims) + FeO(sur) + H_2O(sur) \quad (31)$$

Initial data are provided in Table 1. The algorithm and computational approach used are described in Subheading 2. Acetate permeability was taken to be unidirectional. A proton pump as described in Eq. (26) drives the interior negative relative to the surroundings. Total phosphate in the interior was conserved (i.e., the permeability of phosphate-bearing species was taken to be 0). The transport asymmetry and acetate storage is likely to be a

Table 1

Initial concentrations for simulated species are provided. Values are consistent with those in the literature. The partial pressure of carbon dioxide in the surrounding is taken to be similar to the ambient atmospheric partial pressure (37 Pa). Species X is positively charged and Y is negatively charged and are small ions used to maintain charge neutrality in all compartment interiors

Species	Species #	Surrounding concentrations (M)	Interior concentrations (M)	IMS concentrations (M)
CH_3COOH	1	2.9E-5	1.0E-05	N/A
CH_3COO^-	2	5.0E-3	1.0E-10	N/A
$C_4H_6O_2$	3	N/A	1.0E-10	N/A
CoA^{4-}	4	N/A	5.0E-3	N/A
CH_3COCoA^{4-}	5	N/A	1.0E-10	N/A
ATP^{4-}	6	N/A	8.0E-3	N/A
ADP^{3-}	7	N/A	8.0E-6	N/A
Pi^-	8	N/A	1.0E-7	N/A
NADH	9	N/A	2.86E-6	N/A
NAD^+	10	N/A	2.0E-3	N/A
FeOOH	11	2.0E-2	N/A	N/A
FeO	12	1.0E-10	N/A	N/A
H^+	13	1.0E-7	1.0E-7	1.0E-6
CO_2	14	1.44E-5	1.44E-5	N/A
HCO_3^-	15	6.62E-5	6.62E-5	N/A
X^+	16	5.0662E-3	5.00902005E-2	N/A
Y^-	17	1.0E-7	N/A	N/A
Q(Quinone)	18	N/A	N/A	1.0E-06
QH_2(Quinol)	19	N/A	N/A	1.0E-08
CytocFerrous$^-$	20	N/A	N/A	1.0E-06
CytocFerric	21	N/A	N/A	1.0E-08

natural evolutionary adaptation in the minimal subsurface survival conditions that benefitted *Geobacter* (43). Resulting simulated electrical potentials in the intermembrane space and in the cell interior, relative to the surroundings, are shown in Fig. 1. An initial, short timescale, transient occurred because the overall capacitance of the bacterium's outer membrane (i.e., capacitance/surface area times
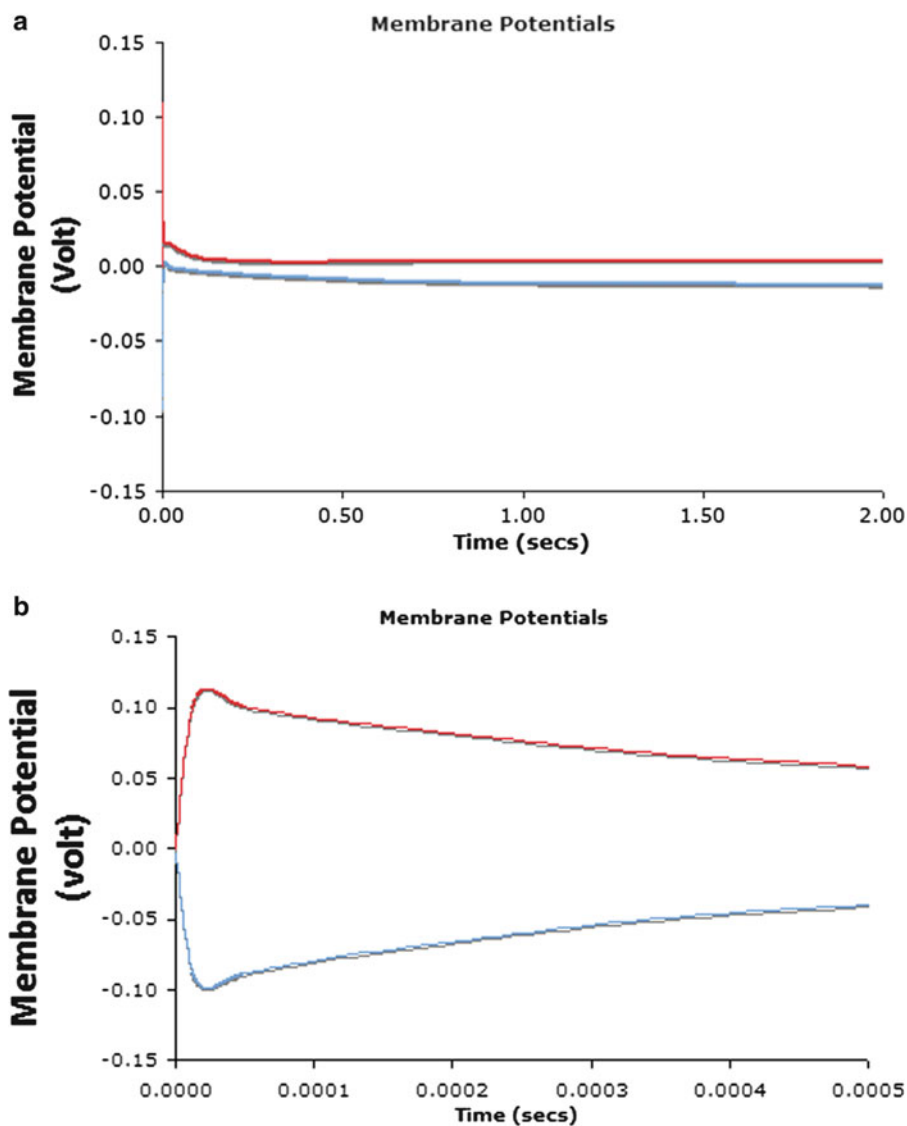
Fig. 1. Membrane potentials for the interior and intermembrane space. The interior potential is measured relative to the intermembrane space. The membrane potential of the outer membrane is that of the intermembrane space minus that of the external medium. These values are on the order of magnitude of those observed (30). (**a**) Full time course showing establishment of a steady state, and (**b**) expanded plot resolving initial transient that takes place on the 50 μs timescale due to the low capacitance of the overall bacterial outer membrane.

surface area) was small due to the size of a bacterium. This is in contrast to the typical response time of a mammalian cell which is on the millisecond timescale.

3.5. Geobacter Fuel Cell *Geobacter sulfurreducens* (*Geobacter* henceforth for simplicity) has been used to create a microbial fuel cell (43–46). The presentation of the E-M network below is organized by following the current
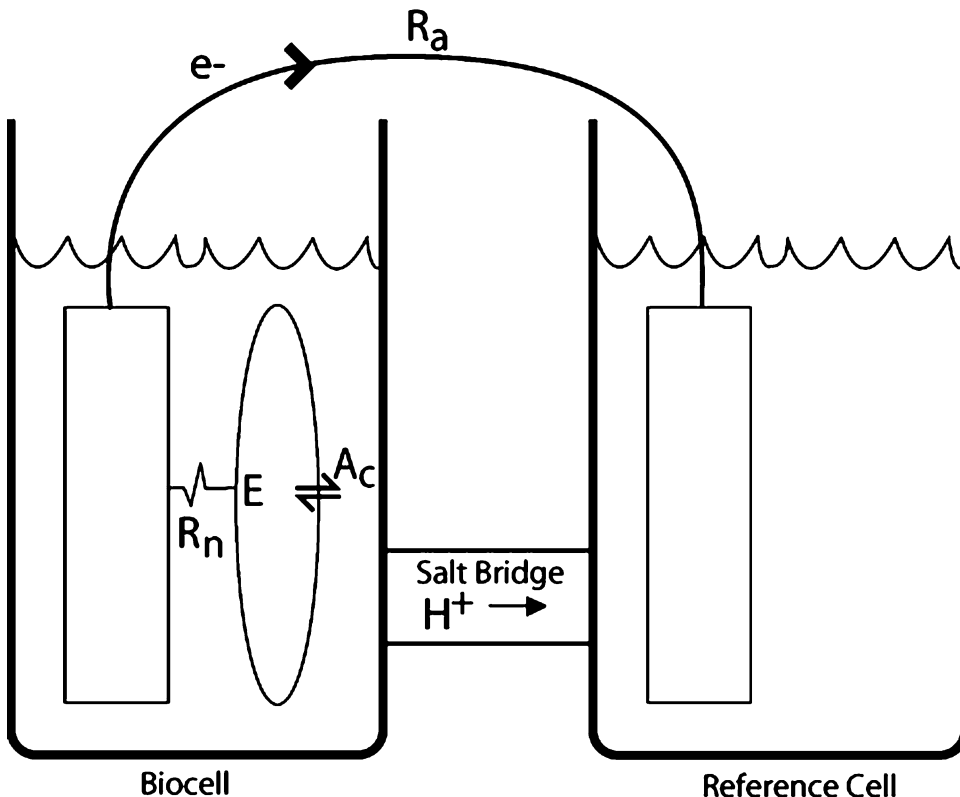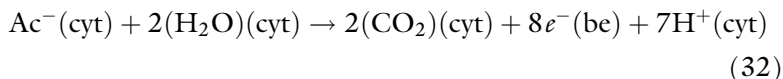
Fig. 2. Schematic microbial fuel cell circuit diagram.

and mass flows around the biofuel cell of Fig. 2. A definition of the variables used is in Tables 2 and 3.

The redox process driving the fuel cell is cast as a transcompartmental reaction that is taken to be the summary process

$$\text{Ac}^-(\text{cyt}) + 2(\text{H}_2\text{O})(\text{cyt}) \rightarrow 2(\text{CO}_2)(\text{cyt}) + 8e^-(\text{be}) + 7\text{H}^+(\text{cyt}) \tag{32}$$

In writing Eq. (32) it is assumed that anodic electron transfer is rapid relative to the rate of the redox process, so that the latter is rate limiting.

This process accounts for the transfer of electrons from the bioelectrode (be) to the reference electrode (re) through the application device, represented by the resistor R_a of Fig. 2, i.e.,

$$e^-(\text{be}) \leftrightarrows e^-(\text{re}) \tag{33}$$

As the electrons reside near the surface of the electrodes, this is a surface-to-surface process (see below).

Charge transfer between the reference electrode and the electrolyte is represented as a transcompartmental reaction

$$2e^-(\text{re}) + 2\text{H}^+(\text{rs}) + (\text{O}_2)(\text{rs}) \leftrightarrows (\text{H}_2\text{O}_2)(\text{rs}) \tag{34}$$
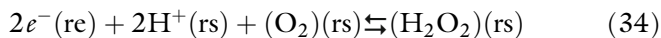
Table 2
Definition of variables

Variable	Definition
V_α	Electrical potential in compartment α
$[\text{species } i]_\alpha$	Activity of molecular component i in compartment α
$c_{i\alpha}$	Molar concentration of molecular component i in compartment α
R_n, R_a	Resistance of the nanowires and application, respectively (Fig. 2)
$\Omega_\alpha, A_{\alpha/\alpha'}$	Volume of compartment α, surface area between compartment α and α'
$C_{\alpha/\alpha'}$	Capacitance of membrane separating α and α'
K_ℓ	Equilibrium constant for process ℓ
F	Faraday's constant
β	$F/R_g T$ for gas constant R_g, absolute temperature T

Table 3
Abbreviations indicate the compartment in which a variable is relevant

| Abbreviation	Definition
be, bs	Bioelectrode, biosolution
re, rs	Reference electrode, reference solution
int	Interior zone within a microbe
PEM	Protein exchange membrane between the bio- and reference solutions
ims	Intermembrane space

As with the redox process within the microbe, a simplified summary reaction is adopted.

This circuit element represents the electrodiffusive flux of protons from the biosolution (bs) to the reference solution (rs) via the cation exchange membrane separating them:

$$H^+(bs) \leftrightharpoons H(rs) \tag{35}$$

It may be possible for other ions and oxygen to diffuse through the membrane; an undesirable decrease in efficiency due to the diffusion of oxygen through the membrane is the decrease in current production of the microbial fuel cell as oxygen can compete with the anode as the final electron acceptor (46), however this was not accounted for in the present study.

In the present minimal network, H^+, K^+, and Ac^- are exchanged across the microbial membrane via the passive process

$$\text{Molecule(bs)}\ddot{\text{A}}\leftrightarrows\text{Molecule(cyt)} \qquad (36)$$
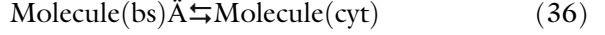
This process is taken to be driven by electrochemical potential differences.

For molecular type i in compartment α, the reaction-transport law is Eq. (1). With the processes presented above, for acetate this takes the form

$$\Omega_{\text{cyt}}\frac{\text{dAc}_{\text{cyt}}^{-}}{\text{d}t} = A_{\text{int/bs}}h_{\text{Ac}^-}\{[\text{Ac}^-]_{\text{bs}} - [\text{Ac}^-]_{\text{cyt}}\} - A_{\text{be/int}}W_1, \quad (37)$$

$$W_1 = k_1[\text{Ac}^-]e^{\beta(V_{\text{be}}-V_{\text{cyt}})} \qquad (38)$$

$A_{\text{be/int}}$ is the cross-section area of the contact between the bacterium (perhaps via nanowires) and the bioelectrode, and $\frac{\beta R_g T}{F} = 1$ for gas constant R and absolute temperature T. The concentration of water is assumed constant, and therefore it is absorbed in the rate coefficient k_1. Note that W_1 is a rate of electron transfer from the cytoplasm to the biosolution.

The following equations complete the E-M model (see Table 3 for abbreviations):

$$C_{\text{re/rs}}\frac{\text{d}}{\text{d}t}(V_{\text{re}} - V_{\text{rs}}) = -A_{\text{re/rs}}W_2 + \frac{V_{\text{re}} - V_{\text{be}}}{FR},$$
$$W_2 = k_2[e^-]_{\text{re}}^2[\text{H}^+]_{\text{rs}}^2[\text{O}_2]_{\text{rs}}, \qquad (39)$$

$$\Omega_{\text{rs}}\frac{\text{dH}_{\text{rs}}^+}{\text{d}t} = -2A_{\text{rs/re}}W_2$$
$$+ A_{\text{PEM}}h_{\text{PEM}}\left\{[\text{H}^+]_{\text{bs}}e^{\beta Z_{\text{H}_{\text{rs}}^+}V_{\text{bs}}} - [\text{H}^+]_{\text{rs}}e^{\beta Z_{\text{H}_{\text{rs}}^+}V_{\text{rs}}}\right\}, \quad (40)$$

$$\Omega_{\text{bs}}\frac{\text{dH}_{\text{bs}}^+}{\text{d}t} = -A_{\text{PEM}}h_{\text{PEM}}\left\{[\text{H}^+]_{\text{bs}}e^{\beta Z_{\text{H}_{\text{rs}}^+}V_{\text{bs}}} - [\text{H}^+]_{\text{rs}}e^{\beta Z_{\text{H}_{\text{rs}}^+}V_{\text{bs}}}\right\}$$
$$+ N_m A_{\text{bs/m}}\hat{J}_{\text{H}^+\text{bs/m}}, \qquad (41)$$

$$C_{\text{m/bs}}\frac{\text{d}}{\text{d}t}[(V_m - V_{\text{bs}})] = A_{\text{m/bs}}F\sum z_i J_{i\text{m/bs}}, \qquad (42)$$

$$C_{\text{be/m}}\frac{\text{d}}{\text{d}t}(V_{\text{be}} - V_m) = -A_{\text{be/m}}W_1, \qquad (43)$$

$$C_{\text{re/be}}\frac{\text{d}}{\text{d}t}(V_{\text{re}} - V_{\text{be}}) = -A_{\text{re/be}}W_1 + \frac{V_{\text{re}} - V_{\text{be}}}{FR}, \qquad (44)$$

$$C_{\text{bs/rs}}\frac{\text{d}}{\text{d}t}(V_{\text{bs}} - V_{\text{rs}}) = \tilde{J}_{\text{H}^+\text{bs/rs}}. \qquad (45)$$

Equations (43), (44), and (39) describe electron transfer from the bacteria to the anode, from the anode to cathode, and from the cathode to the oxygen in the reference solution. Equation (42) models the ionic flux between the representative bacterium and biosolution while Eqs. (40) and (41) describe the temporal evolution of H^+ concentration in the reference and biosolutions, respectively.

In the limit of zero capacitance the differential equation describing the time course of the potential difference between the two electrodes is well approximated by Ohm's law, an algebraic equation relating the voltage to the electrical current, i.e., $V_{re} - V_{be} = IR_a$, where I is the current and R_a is the resistance of the application. However, this limiting behavior is accounted for in our formulation when the value of the capacitance in Eq. (44) is small. There may be a voltage difference between the bioelectrode and the biosolution. However, we assume this potential to be negligible as, in the experiments, bacteria cover more than 75% of the graphite electrode surface (47). Hence, the potential difference between the interior of *Geobacter* and the bioelectrode is equal in magnitude but opposite in sign to the *Geobacter* membrane potential. Connectivity between the bioelectrode and *Geobacter* is established by the different electronic transfer mechanisms mentioned above. An additional compartment whose potential is zero and provides the oxygen needed for the surface reaction producing peroxide in the reference solution was introduced. This compartment defines the potentials along the circuits, since only potential differences are physical.

That *Geobacter* is observed to maintain current even when extracellular acetate levels decrease below the detection limit suggests that there is a mechanism by which *Geobacter* stores acetate or an equivalent substrate internally during a time of acetate abundance in the surroundings. Such a biochemical storage mechanism is confirmed for chemotrophic bacteria that accumulate massive intracellular stores of sudanophilic granules (48–52). These granules consist largely of poly-β-hydroxybyturic acid, $(C_4H_6O_2)_n$ (45). A biochemical storage mechanism has also been discovered for photosynthetic bacteria. For example, the photosynthetic bacterium *Rhodobacter sphaeroides* stores energy by creating a precipitate particle that is consumed after sunset (53, 54). This storage mechanism has the advantage that a relatively insoluble particle can maintain a constant (equilibrium) intracellular substrate level over long periods of time until they are dissolved. In contrast, if the only acetate is that dissolved in the cytoplasm it would be rapidly consumed due to intrabacterial acetate oxidation, and thereby not be available for periods of starvation. We account for this process via a reversible dissolution reaction. This could explain the continuation of *Geobacter* performance in a fuel cell long after acetate levels in the biosolution are depleted. The existence of such a storage mechanism for *Geobacter* has been suggested (55). We have assumed cytoplasmic unidirectional inward membrane transport for acetate ions.

Computer simulations of the equations of Subheading 3 as modified for the fuel cell circuit of Fig. 2 were performed. Experimental values used to calibrate the simulator for the fuel cell are provided in Table 4; biochemical input data and rate constants are summarized in Table 5. A few results are provided in Figs. 3–6. These results suggest that an E-M model could be used to optimize microbial fuel cell performance.

Table 4
Experimental values used in the calibration of parameters found in Table 5 (except for the radius and height for which references are provided)

Species/current	Biosolution (M)	Bioelectrode (mA)	Reference solution (M)	Reference electrode (M)
K^+	0.00334	N/A	0.00134	N/A
Cation	81.66E-03	N/A	57.86E-03	N/A
Anion	85.000158489E-3	N/A	61.200158489E-3	N/A
Ac^-	0.005	N/A	0.0	N/A
H^+	1.58489E-07	N/A	N/A	1.58489E-07
Current	N/A	0.4	N/A	0.

Geobacter sulfurreducens morphology is assumed to be cylindrical (44). Since the current is between the two electrodes, we give the reference electrode a potential of zero so that the difference can be the reported value for the 5 mM-acetate injection experiment (47). Assumed total cation/anion species represent counterbalancing non-permeating ions

Table 5
Calibrated and literature parameters used for *Geobacter*

Parameters	*G. sulfurreducens* ($\mu m, dm^2, nm^2, mL, S^{-1}, L^3 mmol^{-2} S^{-1}, L^5 mmol^{-4} S^{-1}$)
Single cell radius	0.5
Single cell height	0.5
Total surface area between microbes and biosolution	0.459
Total surface area between microbes and bioelectrode	78.54
Volume of biosolution	19.6345409
Intramicrobial storage reaction	$Ac^- \leftrightarrows Ac^*$
$K_{storage}$ (rate constant for the storage reaction)	10
$Q_{storage}$ (equilibrium constant for storage reaction)	1,000
Transcompartmental reaction #1	$Ac^-_{cyt} + 2H_2O_{cyt} \rightarrow 2CO_{cyt} + 7H^+_{cyt} + 8e^-_{be}$
Ktrans1 (rate constant for transcompartmental reaction #1)	1.0 EA
Qtrans1 (equilibrium constant for transcompartmental reaction #1)	5.0×10^{14}
Transcompartmental reaction #2	$2e^-_{rc} + 2H^+_{rs} + O_{2,rs} \rightarrow (H_2O_2)_{rs}$
Ktrans2 (rate constant for transcompartmental reaction #2)	1.0×10^{-10}
Qtrans2 (equilibrium constant for transcompartmental reaction #2)	1.0×10^{35}

The radius and height is used to obtain approximated area and volume assuming cylindrical morphology (44); the area and volume is calculated using data from the literature (47)
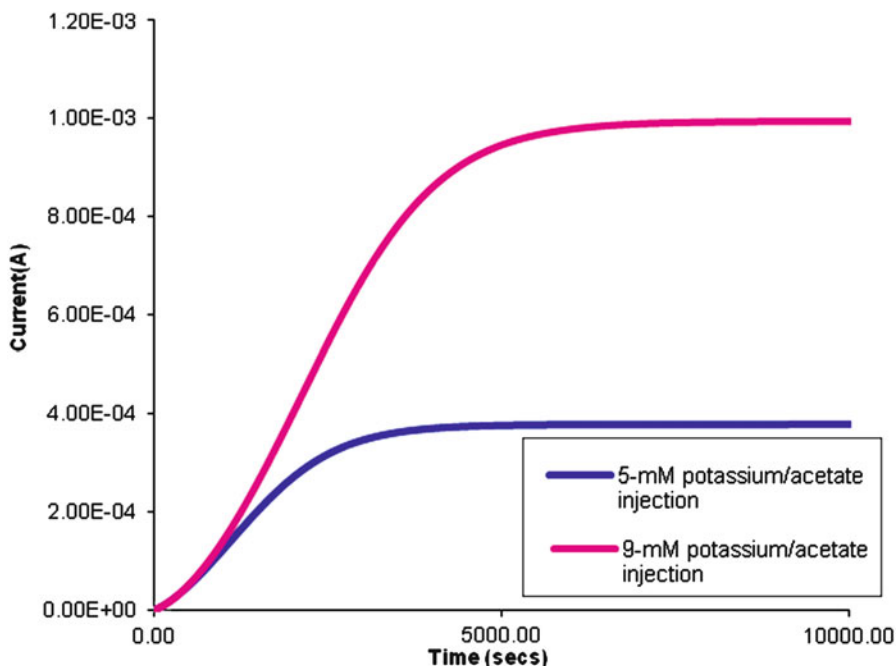
Fig. 3. Responses of the microbial fuel cell generated current to 5 and 9 mM injections of potassium/acetate.
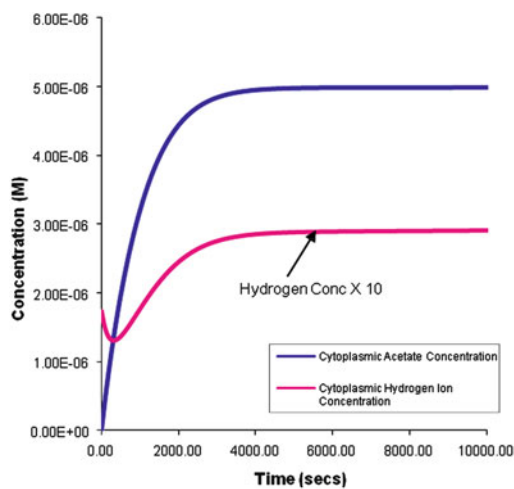

Fig. 4. Response of intra-*Geobacter* acetate and hydrogen ion concentrations following a potassium/acetate injection in the biosolution; hydrogen ion concentration results were multiplied by factor of 10 for visualization.

4. Conclusions

Systems consisting of compartments separated by permeable membranes can exhibit complex phenomena arising through the interplay of reaction and transport processes mediated by electrical
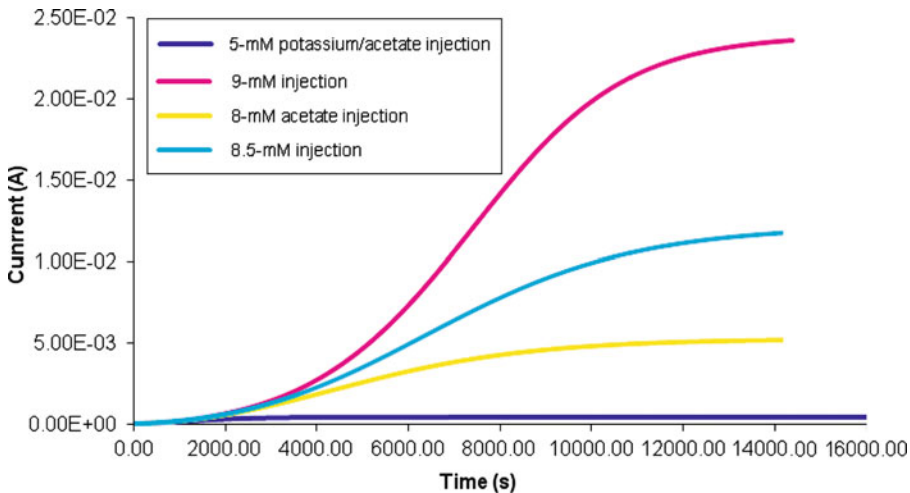
Fig. 5. Response of fuel cell current to acetate injection accompanied by nonpermeant ion for indicated injection concentrations.
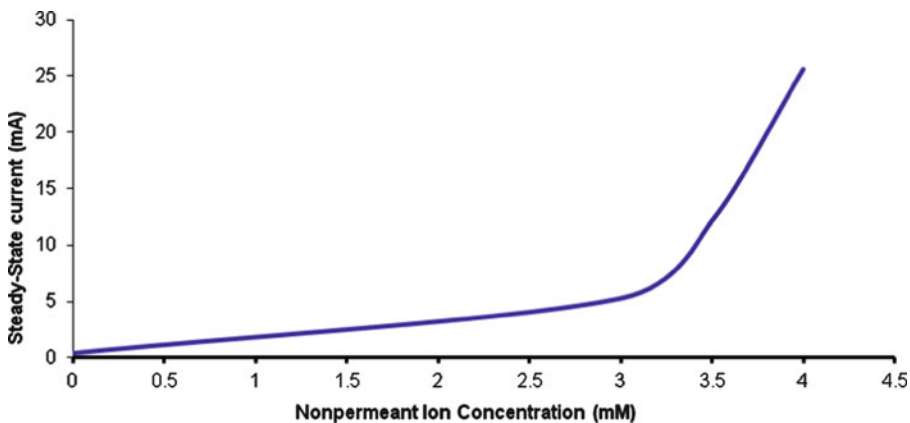

Fig. 6. Dependence of fuel cell steady-state current on nonpermeant ion/acetate injection concentrations.

forces. While strong electrostatic forces constrain the charge density in the interiors of the compartments to near-zero, narrow oppositely charged layers accumulate on each side of the compartment-defining membranes to create transmembrane potentials that mediate the exchange of ions between compartments. A key element of our theory is the partitioning of the transmembrane flux into a component that charges such layers near the membrane surface, and a charge-neutral flux that adds to/subtracts from the bulk within the compartments. As compartment interiors are essentially charge-neutral, the latter component of the membrane flux does not transport net charge. Our formalism is hierarchical, allowing compartments within compartments as in eukaryotic cells or cell aggregates.

The theory reveals the need to develop charge-conserving reaction networks. In contrast to what is commonly presented in the biochemistry literature, the charges of all molecular species must be given and equations charge-balanced. Considering the number of possible states of protonation and other complexing, this is a challenge for self-consistent E-M modeling. Entropy methods show great promise in the latter regard (56, 57). These methods allow for the calibration of incomplete models using uncertain data.

The generality of our formalism makes it applicable to many microbial systems (e.g., bacteria, eukaryotic cells, tissues) and to subsystems in eukaryotic cells (e.g., mitochondria and the nucleus). The present theory with multiplex bioanalytical experimental techniques will, we believe, facilitate the modeling of bioelectric phenomena such as self-organized electrophoresis (13, 58, 59) or patterns of ionic currents that arise in multicellular systems undergoing development or wound healing (13). With this, we believe the present theory holds great promise for attaining quantitative predictions of E-M phenomena.

The examples of Subheading 3 illustrate the potential for using E-M modeling to analyze natural and engineered systems. As our simulator is implemented in a hierarchical fashion, it holds great promise for use as an E-M tissue or organ simulator. This would enhance our understanding of developmental phenomena in single- and multicellular systems (42).

Acknowledgments

References

1. Bakker BM, Michels PA, Opperdoes FR, Westerhoff HV (1997) Glycolysis in bloodstream form *Trypanosoma brucei* can be understood in terms of the kinetics of the glycolytic enzymes. J Biol Chem 272:3207–3215

2. Cortassa S, Aon MA (1994) Metabolic control analysis of glycolysis and branching to ethanol production in chemostat cultures of *Saccharomyces cerevisiae* under carbon, nitrogen, or phosphate limitations. Enzyme Microb Technol 16:761–770

3. Galazzo JL, Bailey JE (1990) Fermentation pathway kinetics and metabolic flux control in suspended and immobilized *Saccharomyces cerevisiae*. Enzyme Microb Technol 12:162–173

4. Garfinkel D, Frenkel RA, Garfinkel L (1968) Simulation of the detailed regulation of glycolysis in a heart supernatant preparation. Comput Biomed Res 2:68–91

5. Baier G, Muller M, Orsnes H (2002) Excitable spatio-temporal chaos in a model of glycolysis. J Phys Chem 106:3275–3282

6. Bakker BM, Mensonides FI, Teusink B, van Hoek P, Michels PA, Westerhoff HV (2000) Compartmentation protects trypanosomes from the dangerous design of glycolysis. Proc Natl Acad Sci U S A 97:2087–2092

7. Eisenthal R, Cornish-Bowden A (1998) Prospects for antiparasitic drugs: the case of *Trypanosoma brucei*, the causative agent of African sleeping sickness. J Biol Chem 273:5500–5505

8. Teusink B, Passarge J, Reijenga CA, Esgalhado E, van der Weijden CC, Schepper M, Walsh MC, Bakker BM, van Dam K, Westerhoff HV, Snoep JL (2000) Can yeast glycolysis be understood in terms of in vitro kinetics of the constituent enzymes? Testing biochemistry. Eur J Biochem 267:5313–5329

9. Zamamiri AM, Birol G, Hjortsø MA (2001) Multiple stable states and hysterisis in continuous, oscillating cultures of budding yeast. Biotechnol Bioeng 73:305–312

10. Navid A, Ortoleva PJ (2004) Simulated complex dynamics of glycolysis in the protozoan parasite *Trypanosoma brucei*. J Theor Biol 228:449–458

11. Weitzke EL, Ortoleva PJ (2003) Simulating cellular dynamics through a coupled transcription, translation, metabolic model. Comput Biol Chem 27:469–481

12. Jaffe LF (1979) Control of development by ionic currents. Soc Gen Physiol Ser 33:199–231

13. Ortoleva P (1981) Developmental bioelectricity. In: Illinger KH (ed) Biological effects of nonionizing radiation. American Chemical Society, Washington, DC, pp 163–212

14. Adebodun F, Post JFM (1993) 19F NMR studies of changes in membrane potential and intracellular volume during dexamethasone-induced apoptosis in human leukemic cell lines. J Cell Physiol 154:199–206

15. London RE, Gabel SA (1989) Determination of membrane potential and cell volume by 19F NMR using trifluoroacetate and trifluoroacetamide probes. Biochemistry 28:2378–2382

16. Miller PGG (1984) Alternate pathways in protozoan energy metabolism. Parasitology 82:23–25

17. Courtemanche M, Ramirez RJ, Nattel S (1998) Ionic mechanisms underlying human atrial action potential properties: insights from a mathematical model. Am J Physiol 275: H301–H321

18. Virgilio L, Bookchin RM (1986) Volume, pH, and ion-content regulation in human red cells: analysis of transient behavior with an integrated model. J Membr Biol 92:57–74

19. Hille B (2001) Ion channels of excitable membranes, 3rd edn. Sinauer Associates, Sunderland

20. Bashford CL, Pasternak CA (1985) Plasma membrane potential of neutrophils generated by the Na$^+$-pump. Biochim Biophys Acta 817:174–180

21. Olschewski A, Hong Z, Nelson DP, Weir EK (2002) Graded response of K$^+$ current, membrane potential, and [Ca2+]i to hypoxia in pulmonary arterial smooth muscle. Am J Physiol Lung Cell Mol Physiol 283:L1143–L1150

22. Leppanen L, Stys PK (1997) Ion transport and membrane potential in CNS myelinated axons II. Effects of metabolic inhibition. J Neurophysiol 78:2095–2107

23. Yasui K, Liu W, Opthof T, Kada K, Lee JK, Kamiya K, Kodama I (2001) I(f) current and spontaneous activity in mouse embryonic ventricular myocytes. Circ Res 88:536–542

24. Terasawa K, Nakajima T, Iida H, Iwasawa K, Oonuma H, Jo T, Morita T, Nakamura F, Fujimori Y, Toyo-oka T, Nagai R (2002) Nonselective cation currents regulate membrane potential of rabbit coronary arterial cell: modulation by lysophosphatidylcholine. Circulation 106:3111–3119

25. Oghalai JS, Zhao HB, Kutz JW, Brownell WE (2000) Voltage- and tension-dependent lipid mobility in the outer hair cell plasma membrane. Science 287:658–661

26. Poberaj I, Rupnik M, Kreft M, Sikdar SK, Zorec R (2002) Modeling excess retrieval in rat melanotroph membrane capacitance records. Biophys J 82:226–232

27. Inoue I, Tsutsui I, Abbott NJ, Brown ER (2002) Ionic currents in isolated and in situ squid Schwann cells. J Physiol 541:769–778

28. Saimi Y, Martinac B, Delcour AH, Minorsky PV, Gustin MC, Culbertson MR, Adler J, Kung C (1992) Patch clamp studies of microbial ion channels. Methods Enzymol 207:681–691

29. Nolan PD, Vooerheis HP (2000) Factors that determine the plasma-membrane potential in bloodstream forms of *Trypanosoma brucei*. Eur J Biochem 267:4615–4623

30. Damper PD, Epstein W (1981) Role of the membrane potential in bacterial resistance to aminoglycoside antibiotics. Antimicrob Agents Chemother 20:803–808

31. Bernstein J (1902) Untersuchungen Zur Thermodynamik der Bioelectrichen Strome. Pfluegers Arch 92:521–562

32. Berstein J (1912) Elektrobiologie. F. Vieweg, Braunschweig

33. Goldman DE (1943) Potential, impedance, and rectification in membranes. J Gen Physiol 27:37–60

34. Hodgkin A, Huxley A (1952) A quantitative description of membrane current and its application to conduction and excitation in nerve. J Physiol 117:500–544

35. Fontus, MWA (2007) Simulating the electrometabolome. Ph.D Thesis, Indiana University, Bloomington. 141 p.

36. Brown PN, Byrne GD, Hindmarsh AC (1989) VODE: a variable coefficient ODE solver. SIAM J Sci Stat Comput 10:1038–1051

37. Byrne GD, Hindmarsh AC (1975) A polyalgorithm for the numerical solution of ordinary differential equations. ACM Trans Math Softw 1:71–96

38. Byrne GD, Hindmarsh AC (1976) EPISODEB: an experimental package for the integration of systems of ordinary differential equations with banded Jacobians. LLNL Report UCID/30132

39. Hindmarsh AC (1983) ODEPACK, a systematized collection of ODE solvers in Scientific Computing. In: R.S. Stepleman et al. (eds.) (vol. 1 of IMACS Transactions on Scientific Computation): North-Holland, Amsterdam, pp. 55–64.

40. Hindmarsh AC, Byrne GD (1977) EPISODE: an effective package for the integration of systems of ordinary differential equations. LLNL Report UCID/30112 1

41. Jackson KR, Sacks-Davis R (1980) An alternative implementation of variable step-size multistep formulas for stiff ODEs. ACM Trans Math Softw 6:295–318

42. Picioreanu C, van Loosdrecht MC, Katuri KP, Scott K, Head IM (2008) Mathematical model for microbial fuel cells with anodic biofilms and anaerobic digestion. Water Sci Technol 57:965–971

43. Logan BE, Hamelers B, Rozendal R, Schröder U, Keller J, Freguia S, Aelterman P, Verstraete W, Rabaey K (2006) Microbial fuel cells: methodology and technology. Environ Sci Technol 40:5181–5192

44. Cord-Ruwisch R, Lovley DR, Schink B (1998) Growth of *Geobacter sulfurreducens* with acetate in syntrophic cooperation with hydrogen-oxidizing anaerobic partners. Appl Environ Microbiol 64:2232

45. Reguera G, Nevin KP, Nicoll JS, Covalla SF, Woodard TL, Lovley DR (2006) Biofilm and nanowire production leads to increased current in *Geobacter sulfurreducens* fuel cells. Appl Environ Microbiol 72:7345

46. Renard F, Gratier JP, Ortoleva P, Brosse E, Bazin B (1998) Self organization during reactive fluid flow in a porous medium. Geophys Res Lett 25:385–388

47. Bond RD, Lovley DR (2000) Electricity production by *Geobacter sulfurreducens* attached to electrodes. Appl Environ Microbiol 69:1548–1555

48. Doodoroff M, Stanier RY (1959) Role of poly-beta-hydroxybutyric acid in aerobic gram-negative bacteria. Nature 183:1440–1442

49. Forsyth WG, Hayward AC, Roberts JB (1958) Occurrence of poly-beta-hydroxybutyric acid in aerobic gram-negative bacteria. Nature 182:800–801

50. Lemoigne M (1927) Etudes sur l'autolyse microbienne. Origine de l'acide-oxybutyrique form'e par autolyse. Ann Inst Pasteur 41:148–165

51. Lemoigne M, Girard H (1943) Reserves lipidiques beta-hydroxybutyriques chez *Azobacter chroococcum*. C R Acad Sci Paris 217:557–558

52. Morris MB, Roberts JB (1959) A group of pseudomonads able to synthesize poly-beta-hydroxybutyric acid. Nature 183:1538–1539

53. Stanier RY (1961) Photosynthetic mechanism in bacteria and plants: development of a unitary concept. Bacteriol Rev 25:1–17

54. Tavano CL, Donahue TJ (2006) Development of the bacterial photosynthetic apparatus. Curr Opin Microbiol 9:625–631

55. Freguia S, Rabaey K, Yuan Z, Keller J (2007) Electron and carbon balances in microbial fuel cells reveal temporary bacterial storage behavior during electricity generation. Environ Sci Technol 41:2915–2921

56. Sayyed-Ahmad A, Tuncay K, Ortoleva PJ (2003) Toward automated cell model development through information theory. J Phys Chem A 107:10554–10565

57. Sayyed-Ahmad A, Tuncay K, Ortoleva PJ (2007) Transcriptional regulatory network refinement and quantification through kinetic modeling, gene expression microarray data and information theory. BMC Bioinformatics 8:20

58. Larter R, Ortoleva P (1981) A theoretical basis for self-electrophoresis. J Theor Biol 88:599–630

59. Larter R, Ortoleva P (1982) A study of instability to electrical symmetry-breaking in unicellular systems. J Theor Biol 96:175–200